Characterization of the Self-Condensation Equilibrium of $[Fe_4S_4(SH)_4]^{2-}$: Spectroscopic Identification of a Unique Sulfido-Bridged Acyclic Tricubane Cluster

H. R. Hoveyda and R. H. Holm*

Department of Chemistry and Chemical Biology, Harvard University, Cambridge, Massachusetts 02138

Received April 9, 1997[⊗]

Our interest in higher nuclearity sulfido-bridged Fe−S clusters, because of their occurrence in several proteins including nitrogenase, prompted us to investigate the solution chemistry of the functionalized cluster $[Fe_4S_4(SH)_4]^{2-}$ (**1**). $(n\text{-}Pr_4N)_2$[**1**] crystallizes in space group $P2_1/n$ of the monoclinic system with $a = 26.201(1)$ Å, $b = 11.4999(5)$ Å, $c = 28.090(1)$ Å, and $\beta = 110.735(1)°$. The X-ray structure reveals the conventional cubane-type geometry with an $[Fe_4S_4]^{2+}$ core symmetry more closely approaching T_d than the tetragonally distorted D_{2d} symmetry reported for the $(PPh_4)_2$[**1**] (Müller, A.; Schladerbeck, N. H.; Bögge, H. *J. Chem. Soc., Chem. Commun.* **1987**, 35). In solution, **1** exists in dynamic equilibrium with self-condensation products formed through elimination of H_2S and formation of sulfido-bridged cluster oligomers, one of which (**4**) is prevalent. The self-condensation equilibrium is shifted toward cluster **1**. When acetonitrile solutions of **1** were treated with thiols more acidic than H_2S, it was possible to detect hydrosulfido terminal ligand substitution products of **1** as well as those of the major self-condensation product **4**. Detailed analysis of the products in acetonitrile solutions of **1**, as well as those generated in solutions of **1** treated with acidic thiol, by electrospray mass spectrometry, and both ^{19}F and ^1H NMR spectroscopy indicates the presence of a sulfido-bridged acyclic trimer of $[Fe_4S_4]^{2+}$ clusters, *i.e.* $\{[Fe_4S_4(SH)_3]_2[Fe_4S_4(SH)_2](\mu\text{-}S)_2\}^{6-}$ (**4**), a hitherto unprecedented Fe−S structural pattern, as the principal Fe−S cluster self-condensation product.

Introduction

Of the myriad of cubane-type iron−sulfur clusters $[Fe_4S_4(SR)_4]^{2-}$ that have been prepared, the species with R = H is the simplest and most fundamental. This cluster was first prepared in 1987 by Müller *et al.*[1] in an apparently serendipitous reaction of $[CpFe(CO)_2I]$ and H_2S and was isolated in 35% yield as the Ph_4P^+ salt. A crystal structure was reported which was described as revealing a tetragonal (D_{2d}) compression of the $[Fe_4S_4]^{2+}$ core, a distortion very common to clusters in this oxidation state.[2] Thereafter, we synthesized this cluster by reaction 1 in acetonitrile in 83% purified yield as the same salt.[3]

$$[Fe_4S_4(SEt)_4]^{2-} + 2H_2S \rightarrow [Fe_4S_4(SH)_4]^{2-} + 4EtSH \quad (1)$$

$$[Fe_4S_4(LS_3)(SEt)]^{2-} + H_2S \rightarrow [Fe_4S_4(LS_3)(SH)]^{2-} \quad (2)$$

$$2[Fe_4S_4(LS_3)(SH)]^{2-} \rightarrow \{[Fe_4S_4(LS_3)]_2S\}^{4-} + H_2S \quad (3)$$

$$2[Fe_4S_4(LS_3)Cl]^{2-} + Li_2S \rightarrow \{[Fe_4S_4(LS_3)]_2S\}^{4-} + 2LiCl \quad (4)$$

The [1:3] site-differentiated cluster in reaction 2 was prepared similarly and obtained in 85−88% yield.[3] In this case, the semirigid trithiolate cavitand ligand LS_3 directs substitution to the unique iron site. Reaction with excess H_2S removes this ligand and affords $[Fe_4S_4(SH)_4]^{2-}$. The occurrence of reaction 3 designates the reactant as a *functionalized* cluster, inasmuch as two hydrosulfide groups condense and eliminate H_2S with formation of a μ-sulfido double cubane.[3] Terminal ligands commonly included in these clusters—thiolate, phenolate, halide—are in general amenable to substitution but require the introduction of a suitable ligand, as in reaction 4,[4] to generate bridged clusters.

While not recurrent, terminal hydrosulfide ligation is nonetheless well established.[5] In addition to the foregoing cases, there are three documented examples of the Fe−SH group, all involving Fe(II).[6−8] Our interest in hydrosulfide clusters is centered in the nature of products obtained by condensation reactions and the attendant possibility of preparing oligomeric iron−sulfur clusters. In the case of reaction 3, only one product is possible. However, the condensation reactions of $[Fe_4S_4(SH)_4]^{2-}$ have a number of conceivable outcomes, including the formation of acyclic and cyclic μ-sulfido oligomers. Such sulfido-bridged assemblies are currently unknown and are of interest with respect to synthetic precursors to the P-cluster of nitrogenase[9] and other polycubane natural products.[10] We report here the results of our initial investigation of the self-condensation reaction of $[Fe_4S_4(SH)_4]^{2-}$ under the conditions of dynamic equilibrium.

[⊗] Abstract published in *Advance ACS Abstracts,* September 1, 1997.

(1) Müller, A.; Schladerbeck, N. H.; Bögge, H. *J. Chem. Soc., Chem. Commun.* **1987**, 35.
(2) Berg, J. M.; Holm, R. H. In *Iron-Sulfur Proteins*; Spiro, T. G., Ed.; Wiley-Interscience: New York, 1982; Chapter 1.
(3) Cai, L.; Holm, R. H. *J. Am. Chem. Soc.* **1994**, *116*, 7177. LS_3 = 1,3,5-tris((4,6-dimethyl-3-mercaptophenyl)thio)-2,4,6-tris(*p*-tolylthio)benzene-(3−).
(4) (a) Stack, T. D. P.; Carney, M. J.; Holm, R. H. *J. Am. Chem. Soc.* **1989**, *111*, 1670. (b) Zhou, C.; Holm, R. H. *Inorg. Chem.* **1997**, *36*, 0000. (c) Huang, J.; Mukerjee, S.; Segal, B. M.; Akashi, H.; Zhou, J.; Holm, R. H. *J. Am. Chem. Soc.*, in press.
(5) Müller, A.; Diemann, E. In *Comprehensive Coordination Chemistry*; Wilkinson, G., Ed.; Pergamon Press: New York, 1987; Vol. 2, Section 16.1.
(6) $[Fe(P(CH_2CH_2PPh_2)_3)(SH)]^+$: Di Vaira, M.; Midollini, S.; Sacconi, L. *Inorg. Chem.* **1977**, *16*, 1518.
(7) $[Fe(dmpe)_2(SH)_2]$: Arif, A. M.; Hefner, J. G.; Jones, R. A.; Koschmieder, S. U. *J. Coord. Chem.* **1991**, *23*, 13.
(8) $[Cp_2Cr_2Fe_2S_4(SH)_2]$: Nefedov, S. E.; Eremenko, I. L.; Pasynskii, A. A.; Yanovskii, A. I.; Struchkov, Yu. T. *Russ. J. Inorg. Chem.* **1992**, *37*, 1402.
(9) (a) Chan, M. K.; Kim, J.; Rees, D. C. *Science* **1993**, *260*, 792. (b) Kim, J.; Woo, D.; Rees, D. C. *Biochemistry* **1993**, *32*, 7104. (c) Peters, J. W.; Stowell, M. H. B.; Soltis, S. M.; Finnegan, M. G.; Johnson, M. K.; Rees, D. C. *Biochemistry* **1997**, *36*, 1181.

S0020-1669(97)00412-6 CCC: $14.00

Experimental Section

Preparations and Reactions. All operations were performed under a pure dinitrogen atmosphere. All solvents were degassed and dried prior to use. 4-Nitrobenzenethiol was prepared as described;[11] other arenethiols were the best commercial products available.

$(n\text{-}Pr_4N)_2[Fe_4S_4(SH)_4]$. In a procedure analogous to that for the $n\text{-}Bu_4N^+$ salt,[3] reaction of 3.00 g (2.30 mmol) of $(n\text{-}Pr_4N)_2[Fe_4S_4(SEt)_4]$[12] and a slight excess of H_2S in acetonitrile solution afforded after workup and drying *in vacuo* 1.81 g (92%) of product as a dark green solid. Absorption spectrum (acetonitrile): λ_{max} (ϵ_M) 266 (24 000), 368 (15 000) nm. ^{1}H NMR (CD_3CN, anion): δ 47.6; other signals are discussed in the text. $E_{1/2} = -1.08$ V (acetonitrile) vs SCE. Anal. Calcd for $C_{24}H_{60}Fe_4N_2S_8$: C, 33.65; H, 7.06; Fe, 26.08; N, 3.27; S, 29.94. Found: C, 33.79; H, 6.94; Fe, 26.21; N, 3.23; S, 29.84.

NMR Samples. Because black precipitates appear in solutions of $[Fe_4S_4(SH)_4]^{2-}$ in a manner dependent on concentration, solvent, and time, the solutions used in the studies that follow were prepared individually *ca.* 15 min before use; all measurements or reactions of these solutions were restricted to 5 h or less. When the concentration range was limited to 5−15 mM, no precipitate was detected in this time period. Ligand substitution reactions were examined using 10 mM solutions of the cluster in acetonitrile to which were added aliquots of 0.4 M stock solutions of arenethiol in acetonitrile. All NMR measurements were made at the ambient probe temperature of 297 K.

Physical Measurements. ^{1}H (400 MHz) and ^{19}F NMR (376 MHz) spectra were recorded on a Bruker AM400 spectrometer; fluorine shifts are referenced to $PhCFCl_2$. For ^{1}H spectra, typically a spectral window of 85 ppm, a pulse angle of 60°, and an acquisition time of *ca.* 0.1 s with a 1 s relaxation delay were employed. For ^{19}F spectra, a spectral window of 9 ppm, a pulse angle of 60°, and an acquisition time of 0.85 s with a 1.5 s delay were used; the time domain for spectral acquisition was commonly set at 5K and was zero-filled to 8K for signal-to-noise improvement. With ^{19}F spectra, an exponential Gaussian line broadening window function was applied to the FID for resolution enhancement prior to Fourier transformation.[13]

Measurement of the redox potential of $[Fe_4S_4(SH)_4]^{2-}$ was made as described elsewhere.[14]

Negative ion electrospray ionization mass spectrometry was carried out using a Platform II mass spectrometer (Micromass Instruments, Danvers, MA). Samples were introduced as acetonitrile solution (*ca.* 500 μM) at a flow rate of 3 μL/min from a syringe pump (Harvard Apparatus). The electrospray probe capillary was maintained at a potential of −3.0 kV and the orifice to skimmer potential (*i.e.* cone voltage, V_c) was varied typically from 10−40 V. Spectra were collected in the multi-channel acquisition mode and were acquired at 5 s/scan and 12 scans were accumulated for each spectrum.

X-ray Structure Determination. Suitable crystals of $(n\text{-}Pr_4N)_2[Fe_4S_4(SH)_4]$ were grown by vapor diffusion of THF into a 1,2-dichloroethane solution. A crystal was transferred to a Siemens SMART diffractometer and cooled to −60 °C in a dinitrogen stream. Initial lattice parameters were obtained by indexing and least-squares analysis of more than 50 centered reflections. A hemisphere of data was collected in the form of 30 s exposure frames with the detector at a distance of 4.90 cm from the crystal. The crystal showed no measurable decay during data collection. The raw intensity data were integrated from frames and converted (including corrections for absorption, background, and Lorentz and polarization effects) to structure factor amplitudes and their esd's. Space group assignment was based on systematic absences and *E* statistics and successful refinement of the structure. The structure was solved by direct methods with the aid of successive difference Fourier maps and refined against all data using the SHELXTL 5.0 software package. Thermal parameters for all non-hydrogen atoms were refined anisotropically. The (SH) hydrogen atoms were not located or included in the refinement; hydrogen atoms associated with the cations were assigned to ideal positions and refined using a riding model with an isotropic thermal parameter 1.2× that of the attached carbon atom (1.5× for the methyl hydrogens). Crystallographic data are collected in Table 1. Selected interatomic distances (Å) and angles (deg) for $[Fe_4S_4(SH)_4]^{2-}$ are collected in Table 2.

Table 1. Crystallographic Data for $(n\text{-}Pr_4N)_2[Fe_4S_4(SH)_4]$

formula	$C_{24}H_{60}FeN_2S_8$
fw	856.62
space group	$P2_1/n$
a (Å)	26.201(1)
b (Å)	11.4999(5)
c (Å)	28.090(1)
β (deg)	110.735(1)
V (Å^3)	7915.6(6)
ρ_{calcd} (g/cm^3)	1.438
T (K)	213
Z	8
μ (mm^{-1})[a]	1.877
$R1$[b]	0.0613
w$R2$[c]	0.1254

[a] Mo Kα radiation (λ = 0.710 73 Å). [b] $R1 = \sum||F_o| - |F_c||/\sum|F_o|$. [c] $wR2 = \{\sum[w(F_o^2 - F_c^2)^2]/\sum[w(F_o^2)^2]\}^{1/2}$.

Results and Discussion

In this investigation, the following clusters are of principal interest. The structure of **1** and possible structures of **2**−**5** are illustrated in Figure 1. Clusters **6**−**8** have been reported previously;[3,15,16] a schematic structure of **6** with the site-differentiating ligand LS_3 is available.[3] Cluster core structure **2** also finds precedent in the literature.[4,17]

$[Fe_4S_4(SH)_4]^{2-}$	**1**[1]
$\{[Fe_4S_4(SH)_3]_2(\mu\text{-}S)\}^{4-}$	**2**
$\{[Fe_4S_4(SH)_2]_2(\mu\text{-}S)_2\}^{4-}$	**3**
$\{[Fe_4S_4(SH)_3]_2[Fe_4S_4(SH)_2](\mu\text{-}S)_2\}^{6-}$	**4**
$\{[Fe_4S_4(SH)_2]_3(\mu\text{-}S)_3\}^{6-}$	**5**
$[Fe_4S_4(LS_3)(SH)]^{2-}$	**6**[3]
$[Fe_4S_4(S\text{-}p\text{-}C_6H_4NO_2)_4]^{2-}$	**7**[15]
$[Fe_4S_4(S\text{-}p\text{-}C_6H_4CF_3)_4]^{2-}$	**8**[16]

Characterization of Cluster 1. The compound $(n\text{-}Pr_4N)_2$[**1**] was prepared by reaction 1 and isolated in 92% yield. Properties sufficient to identify the cluster in solution are summarized in Figure 2. The UV−visible spectrum shows the two-band pattern characteristic of $[Fe_4S_4(SR)_4]^{2-}$ clusters but shifted toward higher energies when compared to typical species such as $[Fe_4S_4(SMe)_4]^{2-}$ (λ_{max} 297, 418 nm in DMF).[15a] These are ligand → core charge transfer transitions; replacement of alkyl with hydrogen in the terminal ligands would be expected to displace the transitions to higher energy, as observed. The reversible redox couple $[\mathbf{1}]^{2-,3-}$ has $E_{1/2} = -1.08$ V, in excellent agreement with the value of −1.10 V predicted from the previously established linear relationship between $[Fe_4S_4(SR)_4]^{2-,3-}$ potentials and Taft σ^* values.[15a] An irreversible band is also observed at *ca.* −1.4 V; this band originates from

(10) (a) Reeve, J. N.; Beckler, G. S.; Cram, D. S.; Hamilton, P. T.; Brown, J. W.; Krzycki, J. A.; Kolodziej, A. F.; Alex, L.; Orme-Johnson, W. H.; Walsh, C. T. *Proc. Natl. Acad. Sci. U.S.A.* **1989**, *86*, 3031. (b) Hedderich, R.; Albracht, S. P. J.; Linder, D.; Koch, J.; Thauer, R. K. *FEBS Lett.* **1992**, *298*, 65. (c) Steigerwald, V. J.; Pihl, T. D.; Reeve, J. V. *Proc. Natl. Acad. Sci. U.S.A.* **1992**, *89*, 6929. (d) Vorholt, J. A.; Vaupel, M.; Thauer, R. K. *Eur. J. Biochem.* **1996**, *236*, 309. These articles describe "polyferredoxins", one of which may contain eight Fe_4S_4 clusters (ref d). These proteins are largely uncharacterized.
(11) Price, C. C.; Stacey, G. W. *J. Am. Chem. Soc.* **1946**, *68*, 498.
(12) Averill, B. A.; Herskovitz, T.; Holm, R. H.; Ibers, J. A. *J. Am. Chem. Soc.* **1973**, *95*, 3523.
(13) Ferrige, A. G.; Lindon, J. C. *J. Magn. Reson.* **1978**, *31*, 337.
(14) Cen, W.; Lee, S. C.; Li, J.; MacDonnell, F. M.; Holm, R. H. *J. Am. Chem. Soc.* **1993**, *115*, 9515.
(15) (a) DePamphilis, B. V.; Averill, B. A.; Herskovitz, T.; Que, L., Jr.; Holm, R. H. *J. Am. Chem. Soc.* **1974**, *96*, 4159. (b) Que, L., Jr.; Bobrik, M. A.; Ibers, J. A.; Holm, R. H. *J. Am. Chem. Soc.* **1974**, *96*, 4168.
(16) Wong, G. B.; Kurtz, D. M., Jr.; Holm, R. H.; Mortenson, L. E.; Upchurch, R. G. *J. Am. Chem. Soc.* **1979**, *101*, 3078.
(17) $(Bu_4N)_2(PPh_4)_2[(Fe_4S_4Cl_3)_2(\mu\text{-}S)]$: Challen, P. R.; Koo, S.-M.; Dunham, W. R.; Coucouvanis, D. *J. Am. Chem. Soc.* **1990**, *112*, 2455.

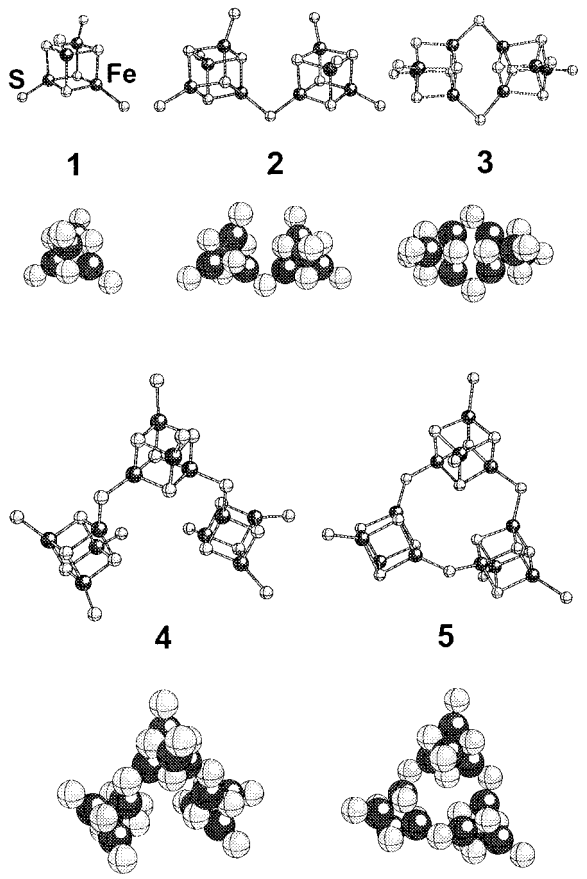

Figure 1. Ball-and-stick and space-filling depictions of $[Fe_4S_4(SH)_4]^{2-}$ (**1**) and its possible self-condensation products with one (**2**, **3**) and two (**4**, **5**) additional clusters.

Table 2. Selected Interatomic Distances (Å) and Angles (deg) for $[Fe_4S_4(SH)_4]^{2-}$

Fe(1)−S(1)	2.287(2)	Fe(1)−Fe(2)	2.789(1)
Fe(1)−S(2)	2.306(2)	Fe(1)−Fe(3)	2.769(1)
Fe(1)−S(4)	2.286(4)	Fe(1)−Fe(4)	2.769(1)
Fe(2)−S(1)	2.290(2)	Fe(2)−Fe(3)	2.768(1)
Fe(2)−S(2)	2.283(2)	Fe(2)−Fe(4)	2.771(1)
Fe(2)−S(3)	2.290(2)	Fe(3)−Fe(4)	2.753(1)
Fe(3)−S(1)	2.291(2)	mean of 6	2.77(1)
Fe(3)−S(3)	2.292(2)		
Fe(3)−S(4)	2.273(2)	Fe(1)−S(5)	2.207(2)
Fe(4)−S(2)	2.299(2)	Fe(2)−S(6)	2.209(2)
Fe(4)−S(3)	2.271(2)	Fe(3)−S(7)	2.214(2)
Fe(4)−S(4)	2.287(2)	Fe(4)−S(8)	2.211(2)
mean of 12	2.288(9)	mean of 4	2.210(3)
(μ_3-S)−Fe−(μ_3-S)			
range		102.71−104.12	
mean of 12		103.6(4)	
Fe−(μ_3-S)−Fe			
range		73.93(6)−75.09(5)	
mean of 12		74.5(3)	
Fe−Fe−Fe (range)		59.60(3)−60.26(3)	
(μ_3-S)−Fe−S(n) (range)		112.48(8)−118.04(7) (n = 5−8)	

the H_2S present in solution (Figure 2). The cluster exhibits a strong ^{1}H NMR signal whose shift is markedly solvent dependent. For example, at 297 K this signal occurs at 47.6 ppm in acetonitrile, shown in Figure 3A, and at 64.5 ppm in pyridine. A corresponding signal for the mono(hydrosulfide) cluster **6** is found at 46.5 ppm in acetonitrile.[3] Addition of a slight amount of D_2O abolishes the signals. These resonances arise from the −SH proton and are not excessively broadened ($\omega_{1/2} \approx 70$ Hz) despite being only two bonds removed from an iron atom. The additional SH resonances in Figure 3A are discussed below. In acetonitrile, the isotropic (contact) shift $(\Delta H/H_0)_{iso} = (\Delta H/H_0)_{dia} - (\Delta H/H_0)_{obs} = -51.4$ ppm for **1** (relative to Et_4NSH at −3.84 ppm). The isotropic shifts of **1** and **6**[3] are practically linear

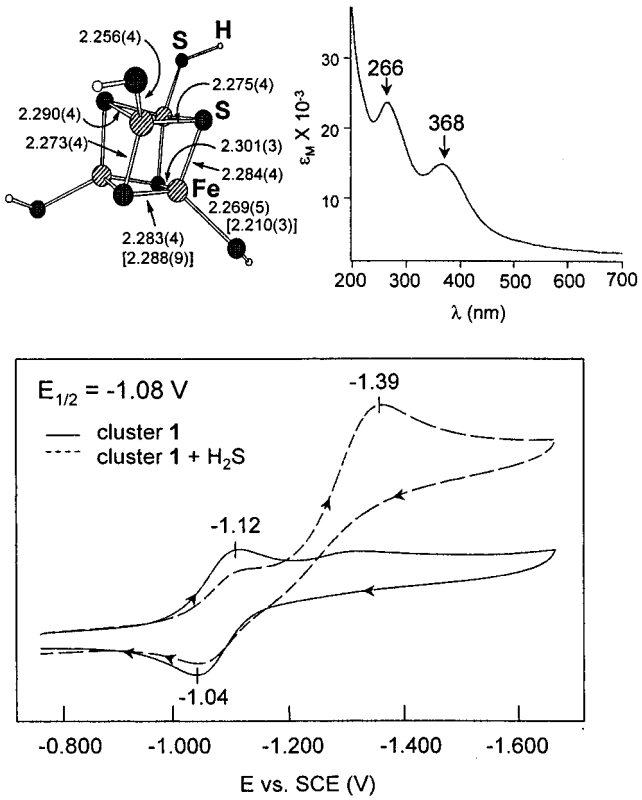

Figure 2. Properties of $[Fe_4S_4(SH)_4]^{2-}$ (**1**): X-ray structure, including bond lengths (Å) from an earlier determination[1] and mean values (brackets) from this work; absorption spectrum in acetonitrile; cyclic voltammogram in the presence and absence of added H_2S in acetonitrile solution (0.1 M (n-Bu_4N)(PF_6) supporting electrolyte, 50 mV/s, $E_{1/2}$ = −1.08 V vs SCE).

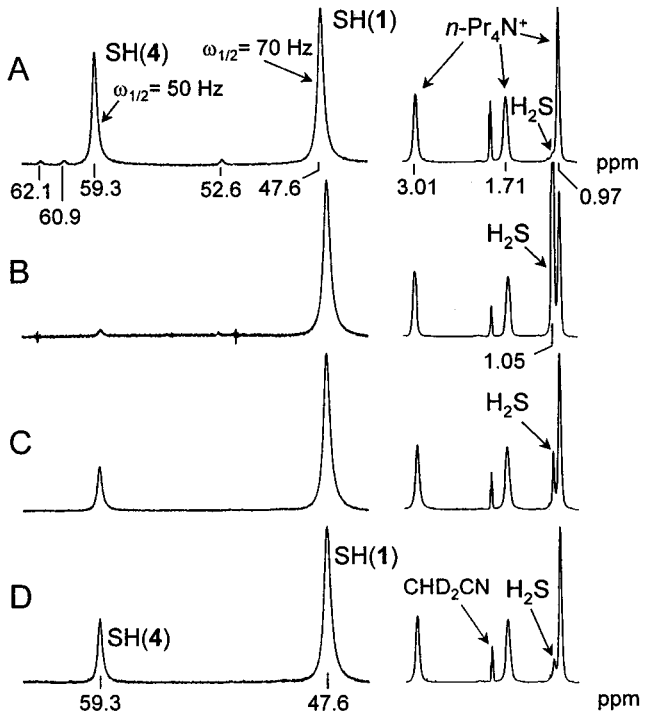

Figure 3. ^{1}H NMR spectra of $[Fe_4S_4(SH)_4]^{2-}$ (**1**, 10 mM) in CD_3CN solution (A), in a saturated solution of H_2S (B), and in solutions from which H_2S was removed by freeze−pump−thaw cycles (C, D). The signal of **1** is indicated in spectrum A. The concentration of $[Fe_4S_4]^{2+}$ cores in all species is 10 mM. The SH(**4**) resonance arises from an oligomeric cluster (see text).

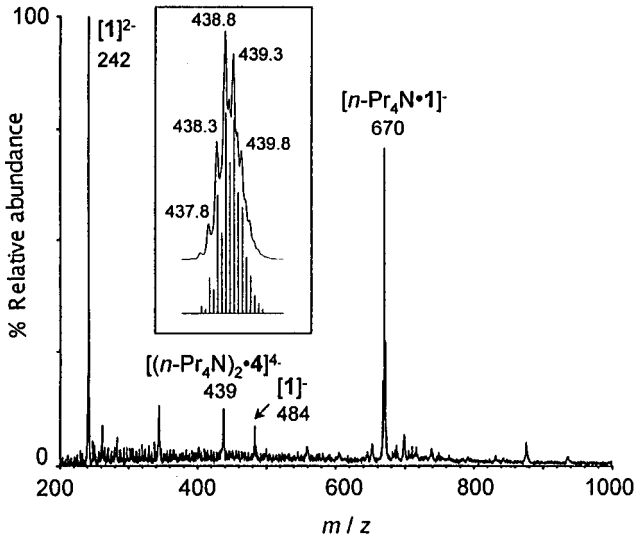

Figure 4. Negative ion ESMS of $(n\text{-}Pr_4N)_2[Fe_4S_4(SH)_4]$. The spectrum was recorded using a 0.5 mM solution in acetonitrile. The insert shows the peak at $m/z = 439$ in magnification with the calculated isotope pattern for $[(n\text{-}Pr_4N)_2\cdot\mathbf{4}]^{4-}$ ($m/z = 439$) indicated with bars (see text).

with $1/T$ and increase with increasing temperature (not shown). These features are consistent with a contact interaction and the thermal population of an excited paramagnetic state, the consistent behavior of clusters with the $[Fe_4S_4]^{2+}$ oxidation state and an $S = 0$ ground state.

The negative ion ESMS[18] of an acetonitrile solution of **1** is shown in Figure 4. Evident in the mass spectrum is the base ion at $m/z = 242$, which corresponds to the doubly charged $[\mathbf{1}]^{2-}$ species (isotope peaks separated by 0.5 m/z unit[19]); the second most intense peak is assigned to the singly charged ion $[n\text{-}Pr_4N\cdot\mathbf{1}]^-$ based on mass isotope pattern and isotope peak separation criteria. The relative abundance and the extent of fragmentation of these ions is highly dependent on the sampling cone voltage (V_c) employed.[20] The additional ion at $m/z = 439$ in Figure 4 is discussed below.

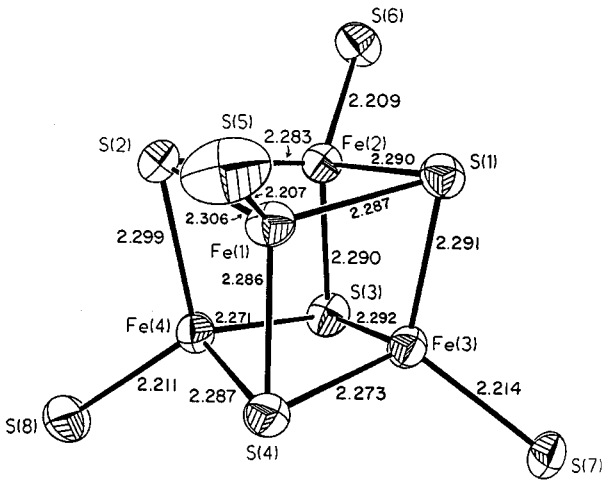

Figure 5. Structure of $[Fe_4S_4(SH)_4]^{2-}$ (**1**, cluster 1) showing the atom-labeling scheme, selected bond distances (Å), and 40% probability ellipsoids.

The X-ray structure of **1** reveals the conventional cubane-type geometry associated with clusters of the type $[Fe_4S_4L_4]^{z-}$.[2,25] There are two clusters in the asymmetric unit; because they are virtually isodimensional, only cluster 1 is depicted in Figure 5, and the metric data in Table 2 are limited to those of this cluster. Because of the similarity to previous $[Fe_4S_4(SR)_4]^{2-}$ structures, no extensive discussion of the present structure is warranted. We note, however, several points of interest. (i) Neither cluster 1 nor 2 shows the compressed tetragonal distortion, with four short Fe−S bonds roughly parallel to an idealized $\bar{4}$ axis. Instead, bond lengths differ by a maximum of 0.035 Å in cluster 1 and 0.018 Å in cluster 2 and there is no discernible pattern of long and short bonds. While no symmetry is imposed, the cluster cores more closely approach T_d than D_{2d} symmetry. The spread of Fe−S distances in the Ph_4P^+ salt (imposed C_2 symmetry) is only 0.028 Å, and despite a statement to the contrary,[1] there is no clear tetragonal distortion. (ii) The Fe−SH distances in the $n\text{-}Pr_4N^+$ (Table 1) and Ph_4P^+ salts are decidedly different. The mean values in clusters 1 and 2 are 2.210(3) and 2.208(8) Å, respectively, while the values in the Ph_4P^+ salt are 2.269(5) and 2.256(4) Å.[1] A difference of $\gtrsim$0.04 Å in terminal Fe−SR distances at parity of R is usually associated with differences in oxidation state, but that is not the case here. We cannot satisfactorily explain the difference in Fe−SH bond lengths in the two salts of **1**. Despite the latter feature, we conclude that **1** is a standard $[Fe_4S_4]^{2+}$ cluster in all respects except reactivity, as the results in the sections that follow reveal.

Terminal Ligand Substitution Reactions. $[Fe_4S_4(SH)_4]^{2-}$. In solutions of **1**, there occur, in addition to the SH(**1**) resonance, other signals. The resonance at 59.3 ppm ($\omega_{1/2} \approx 50$ Hz) in

(18) For general reviews on electrospray ionization mass spectrometry (ESMS) see: (a) Fenn, J. B.; Mann, M.; Meng, C. K.; Wong, S. F.; Whitehouse, C. M. *Science* **1989**, *246*, 64. (b) Smith, R. D.; Loo, J. A.; Edmonds, C. G.; Barinaga, C. J.; Udseth, H. R. *Anal. Chem.* **1990**, *62*, 882. (c) Przybylski, M.; Glocker, M. O. *Angew. Chem., Int. Ed. Engl.* **1996**, *35*, 806. For application of ESMS to Fe−S proteins see: (d) Pétillot, Y.; Forest, E.; Meyer, J.; Moulis, J.-M. *Biochem. J.* **1995**, *296*, 657. (e) Pétillot, Y.; Forest, E.; Meyer, J.; Moulis, J.-M. *Anal. Biochem.* **1995**, *228*, 56.

(19) For the use of $^{12}C/^{13}C$ isotope peak spacing to adduce z, see: Henry, K. D.; McLafferty, F. W. *Org. Mass Spectrom.* **1990**, *25*, 490.

(20) This phenomenon has been amply reported in the literature.[21] We observed that at $V_c \leq 25$ V the $m/z = 242$ signal consists of both −2 and −1 ions whereas at $V_c \geq 50$ V a singly charged fragment, $[Fe_2S_2(SH)_2]^-$, prevails.

(21) (a) Katta, V.; Chowdhury, S. K.; Chait, B. T. *J. Am. Chem. Soc.* **1990**, *112*, 5348. (b) Leize, E.; Van Dorsselaer, A.; Krämer, R.; Lehn, J.-M. *J. Chem. Soc., Chem. Commun.* **1993**, 990 and references therein. (c) van den Bergen, A.; Colton, R.; Percy, M.; West, B. O. *Inorg. Chem.* **1993**, *32*, 3408. (d) Kane-Maguire, L. A. P.; Kanitz, R.; Sheil, M. M. *J. Organomet. Chem.* **1995**, *486*, 243.

(22) A peak of lower intensity (≤10%) is detected at $m/z = 484$ which is attributable to the oxidized $[\mathbf{1}]^-$ species (Table 3). While we do not purport to have examined extensively the cause of formation of this oxidized species in the ESMS, we note that the negative ion ESMS of a conventional cluster such as $[Fe_4S_4(SEt)_4]^{2-}$, obtained under identical conditions, also displayed a similar feature. Thus it seems rather likely that this oxidized cluster species is formed by the presence of residual amounts of O_2 in the nebulizer gas employed (*viz.* N_2 or standard air mixture). When Ar was used as the nebulizer gas, the negative ion ESMS could not be obtained presumably due to the well-known problem of corona discharge,[23] which may be remedied by the presence of an electron scavenger such as O_2[24a] or SF_6,[24b] as has been documented previously.

(23) The electric (corona) discharge phenomenon is caused by electrons emanating from the sharp edges of the ES needle held at a few thousand volts negative relative to a counter-electrode. See: (a) Cole, R. B.; Harrata, A. K. *J. Am. Mass Spectrom.* **1993**, *4*, 546. (b) Straub, R. F.; Voyksner, R. D. *J. Am. Mass Spectrom.* **1993**, *4*, 578.

(24) (a) Yamashita, M.; Fenn, J. B. *J. Phys. Chem.* **1984**, *88*, 4671. (b) Ikonomou, M. G.; Blades, A. T.; Kebarle, P. J. *J. Am. Mass Spectrom.* **1991**, *2*, 497. The use of sharpened ES capillary tips has also been suggested as an alternative solution: (c) Chowdhury, S.; Chait, B. T. *Anal. Chem.* **1991**, *673*, 1660.

(25) (a) Carney, M. J.; Papaefthymiou, G. C.; Spartalian, K.; Frankel, R. B.; Holm, R. H. *J. Am. Chem. Soc.* **1988**, *110*, 6084 and references therein. (b) Carney, M. J.; Papaefthymiou, G. C.; Frankel, R. B.; Holm, R. H. *Inorg. Chem.* **1989**, *28*, 1497, and references therein. (c) Excoffon, P.; Laugier, J.; Lamotte, B. *Inorg. Chem.* **1991**, *30*, 3075. (d) Evans, D. J.; Hills, A.; Hughes, D. L.; Leigh, G. J.; Houlton, A.; Silver, J. *J. Chem. Soc., Dalton Trans.* **1990**, 2735.

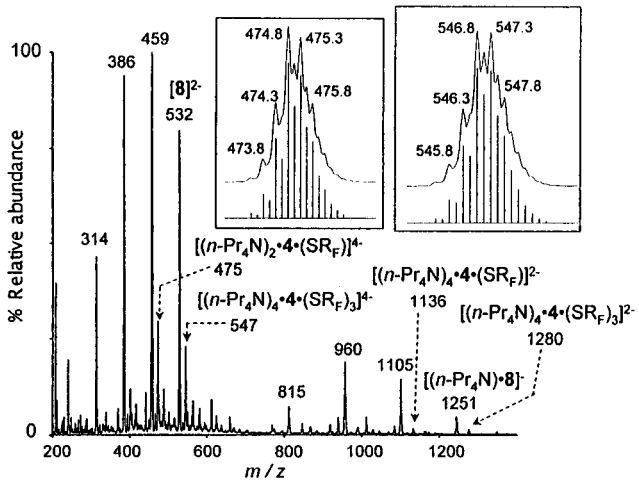

Figure 6. Negative ion ESMS of $(n\text{-}Pr_4N)_2[Fe_4S_4(SH)_4]$ + 2 equiv of $p\text{-}CF_3C_6H_4SH$. The spectrum was recorded using a 0.5 mM solution in acetonitrile. The insert shows the peaks at m/z = 475 and m/z = 547 in magnification with the calculated isotope pattern for $\{(n\text{-}Pr_4N)_2\cdot[\mathbf{4}\cdot(SR_F)_1]\}^{4-}$ (m/z = 475) and $\{(n\text{-}Pr_4N)_2\cdot[\mathbf{4}\cdot(SR_F)_3]\}^{4-}$ (m/z = 547) indicated with bars. See Table 4 for peaks corresponding to $[\mathbf{1}\cdot(SR_F)_n]$ species.

Figure 3A, designated SH(**4**), accounts for *ca.* 35% of the total integrated intensity of SH resonances, while the three minor features in the 52−62 ppm region altogether account for ≤5% of the total integrated signal intensity[26] (*cf.* Figure 3A). All of these resonances are eliminated by addition of trace D_2O and are therefore assigned to SH protons. Further a weak shoulder occurs at 1.05 ppm which is due to H_2S. When the solution is saturated with H_2S, the SH(**4**) resonance is greatly suppressed and the minor signals are hardly detectable (Figure 3B). Depletion of H_2S results in the re-emergence of the SH(**4**) signal (Figure 3C,D). *Thus the two major cluster species (one of which is cluster* ***1****) and H_2S are coupled in a reversible equilibrium.*

To search out further information regarding the *second* major cluster species, that affording the SH(**4**) signal at 59.3 ppm, a number of terminal ligand substitution studies were undertaken. Electrospray mass spectrometry (ESMS) as well as ^{19}F and ^1H NMR spectroscopy were employed to analyze the substitution products of the two major cluster species (*vide infra*). Of relevance to this aspect of the present investigation is the observation of an m/z = 439 peak in the negative ion ESMS of cluster **1** in acetonitrile (Figure 4 and its inset). Comparison of the calculated *versus* observed mass isotope pattern corroborates its assignment as the sulfido-bridged tricubane $[(n\text{-}Pr_4N)_2\cdot\mathbf{4}]^{4-}$ ion. Further evidence which implicates cluster **4** as the second major cluster species is presented below.

(a) 1 + *p*-$CF_3C_6H_4SH$: ESMS Studies. The negative ion ESMS of an acetonitrile solution of cluster **1** with 1, 2, and 3 equiv of $p\text{-}CF_3C_6H_4SH$ (R_FSH) was examined. Displayed in Figure 6 is a representative example of one such study which clearly reveals the presence of the $[Fe_4S_4(SH)_{4-n}(SR_F)_n\cdot x Pr_4N]^{x-2}$ species, where n = 1−4 and x = 0, 1. Species detected and their relative intensities are listed in Table 4. These species are generated by the terminal ligand substitution of cluster **1**. Under mild conditions ($V_c \leq 20$ V), the ESMS results agree with the ^{19}F NMR findings inasmuch as the relative intensities of the 2− ions in the mass spectrum—*i.e.*, $n(m/z)$: 1(314); 2(386); 3(459); 4(532)—parallel the relative integrated intensity for the same species in the NMR spectrum (*cf.* Figures 6 and 7). At higher cone voltages ($V_c \geq 20$ V), however, the more substituted species predominate in the mass spectrum (not shown), and as such, the distribution of the terminal ligand substituted species no longer matches the trend observed in the NMR spectrum.

Table 3. Electrospray Mass Spectral Data for Cluster **1** in Acetonitrile

cluster species	ion	peak (m/z)	rel intensity (%)
1	$[\mathbf{1}]^{2-}$	241.8	100
	$[\mathbf{1}]^{1-}$	483.6[a]	8
	$[(n\text{-}Pr_4N)\cdot\mathbf{1}]^{-}$ [a]	669.9	75
4	$[(n\text{-}Pr_4N)_2\cdot\mathbf{4}]^{4-}$	438.8	12

[a] See ref 22.

Table 4. Electrospray Mass Spectral Data for Cluster **1** and 2 equiv of $p\text{-}CF_3C_6H_4SH$ in Acetonitrile

cluster species	ion[a]	peak (m/z)	rel intensity (%)
1	$[\mathbf{1}\cdot(SR_F)]^{2-}$	313.6	56
	$\{(n\text{-}Pr_4N)\cdot[\mathbf{1}\cdot(SR_F)_1]\}^{-}$	814.8	7
	$[\mathbf{1}\cdot(SR_F)_2]^{2-}$	385.8	94
	$\{(n\text{-}Pr_4N)\cdot[\mathbf{1}\cdot(SR_F)_2]\}^{-}$	959.6	30
	$[\mathbf{1}\cdot(SR_F)_3]^{2-}$	458.6	100
	$\{(n\text{-}Pr_4N)\cdot[\mathbf{1}\cdot(SR_F)_3]\}^{-}$	1105.2	20
	$[\mathbf{1}\cdot(SR_F)_4]^{2-}$ (≡ $\mathbf{8}^{2-}$)	532.1	80
	$\{(n\text{-}Pr_4N)\cdot[\mathbf{1}\cdot(SR_F)_4]\}^{-}$	1250.7	7
4	$\{(n\text{-}Pr_4N)\cdot[\mathbf{4}\cdot(SR_F)_1]\}^{5-}$	342.1	5
	$\{(n\text{-}Pr_4N)_2\cdot[\mathbf{4}\cdot(SR_F)_1]\}^{4-}$	475.3	42
	$\{(n\text{-}Pr_4N)_4\cdot[\mathbf{4}\cdot(SR_F)_1]\}^{2-}$	1136.5	5
	$\{(n\text{-}Pr_4N)\cdot[\mathbf{4}\cdot(SR_F)_2]\}^{5-}$	371.6	8
	$\{(n\text{-}Pr_4N)\cdot[\mathbf{4}\cdot(SR_F)_3]\}^{5-}$	400.3	15
	$\{(n\text{-}Pr_4N)_2\cdot[\mathbf{4}\cdot(SR_F)_3]\}^{4-}$	547.3	33
	$\{(n\text{-}Pr_4N)_4\cdot[\mathbf{4}\cdot(SR_F)_3]\}^{2-}$	1279.6	4
	$\{(n\text{-}Pr_4N)_2\cdot[\mathbf{4}\cdot(SR_F)_4]\}^{4-}$	583.2	12
	$\{(n\text{-}Pr_4N)_2\cdot[\mathbf{4}\cdot(SR_F)_5]\}^{4-}$	619.2	7
	$\{(n\text{-}Pr_4N)\cdot[\mathbf{4}\cdot(SR_F)_7]\}^{5-}$	515.7	5
	$[\mathbf{4}\cdot(SR_F)_8]^{6-}$	422.0	4
	$\{(n\text{-}Pr_4N)_3\cdot[\mathbf{4}\cdot(SR_F)_8]\}^{3-}$	1031.6	5

[a] $[\mathbf{1}\cdot(SR_F)_n] \equiv [Fe_4S_4(SH)_{4-n}(SR_F)_n]^{2-}$. Similarly, $[\mathbf{4}\cdot(SR_F)_n]$ symbolizes cluster **4** with n R_FS^- ligands replacing n HS^- ligands.

In addition to terminal ligand-substituted cluster **1** species, a series of peaks attributable to substituted cluster **4** species was also detected (Table 4). Several of this latter group of signals are labeled in Figure 6. These observations lend further support to the aforementioned ESMS evidence (*i.e.*, the m/z = 439 peak in Figure 4). Depicted in Figure 6 (insets) are two examples of the peak assignment verification for the substituted cluster **4** species.

The relative abundance of the cluster **4** substituted species in the ESMS is always appreciably less than the analogous cluster **1** species, similar to the observation in the NMR spectra. However, it is important to point out that the relative peak intensities reported in Tables 3 and 4 are unlikely to be a direct measure of the relative equilibrium concentrations of species **1** and **4**. This is based on the following principal considerations. (i) The efficiency of the transfer of complex ions into the gas phase has been recognized to depend on their charge state.[27] (ii) The effect of applying high voltages, requisite for formation of an ion spray,[18a−c] on the relative concentration of equilibrium species cannot be accounted for. (iii) The solutions employed in ESMS studies (≤0.5 mM) are 20-fold less concentrated than the NMR samples employed (10 mM).

(b) 1 + *p*-$CF_3C_6H_4SH$: ^{19}F NMR Studies. The sensitivity of the isotropically shifted ^{19}F (and ^1H) resonances of substituted

(26) The minor species corresponding to the three very weak features in Figure 3A, other than being $[Fe_4S_4]^{2+}$ clusters on the basis of chemical shift, have not been identified and are not considered further.

(27) Andersen, U. N.; McKenzie, C. J.; Bojesen, G. *Inorg. Chem.* **1995**, *34*, 1435.

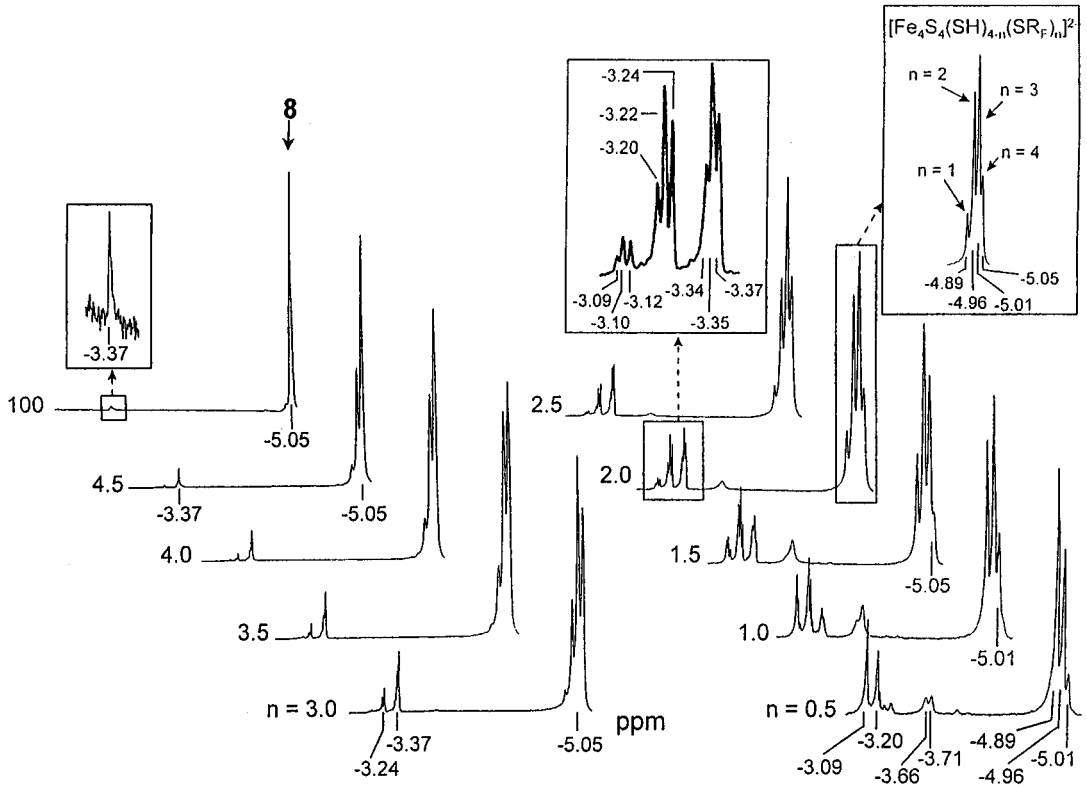

Figure 7. ^{19}F NMR spectral changes (376 MHz) caused by the addition of *n* equiv of *p*-$CF_3C_6H_4SH$ to a CD_3CN solution of $[Fe_4S_4(SH)_4]^{2-}$ (**1**) at ambient temperature. Note that inset spectra are expanded portions of spectra at $n = 100$ equiv (left) and $n = 2.0$ equiv (center, right).

ligands at the Fe site to the type of cluster, composition of the *total* ligand set, and the respective attendant symmetry of the clusters upon terminal ligand substitution is a property of prime importance to this investigation. Numerous examples of this behavior have been previously presented.[16,28] Here, this property is utilized in order to examine further the identity of the second major cluster species.

As with the case of thiolate ligand substitution, terminal hydrosulfide substitution of $[Fe_4S_4(SH)_n]^{2-}$ also occurs *via* stepwise reversible equilibria ($n = 1-4$), and at fixed *n* it has the characteristic of an acid-base reaction.[29] The only caveat in the latter case is that the thiol used to substitute the terminal hydrosulfido moieties must be more acidic than H_2S, the conjugate acid byproduct (aqueous $pK_a = 7.02$[30]); *p*-$CF_3C_6H_4$-SH (estimated aqueous $pK_a = 5.6$[31]) fulfills this requirement. Furthermore, this acidic fluorinated arenethiol also provides the best ^{19}F chemical shift resolution for the reasons elaborated elsewhere.[16]

Two groups of ^{19}F signals are observed in the NMR spectra within a 2 ppm window (Figure 7). The group with larger integrated intensities is comprised of a total of four ^{19}F signals with chemical shift values at *ca.* −5 ppm and is thus assigned as the $[Fe_4S_4(SH)_{4-n}(SR_F)_n]^{2-}$ resonances.[16] On the basis of growth and decay of their relative integrated intensities, these four signals can be assigned as follows: −4.89 ppm, $n = 1$; −4.96 ppm, $n = 2$; −5.01 ppm, $n = 3$; and −5.05 ppm, $n = 4$ (**8**). The relative distribution of these substituted species as observed in ESMS spectrum correlates with that in the ^{19}F NMR spectrum (*cf.* Figure 7, $n = 2.0$).

A more complex group of ^{19}F resonances is also observed within a *ca.* 0.6 ppm spectral window and centered near 3.2 ppm. Under optimized resolution conditions, a total of 11 ^{19}F resonances can unambiguously be observed spanning a range from −3.09 to −3.71 ppm. When the ^{19}F NMR spectra were obtained at a different magnetic field (282 MHz), the chemical shifts (ppm) were observed to be identical whereas the ^{19}F peak separation (Hz) were smaller in each case. The 11 ^{19}F resonances are therefore *not* due to long range $\{^1H,^{19}F\}$ coupling and are engendered by at least *11* inequivalent ^{19}F nuclei.

The relative integrated intensities of the two groups of ^{19}F resonances (for $n = 0.5$ and $n = 1.0$) matches the observed ratios for SH(**1**) and SH(**4**) ^{1}H NMR signals (Figure 3) within 5%. Moreover, the growth and decay of this group of (11) ^{19}F resonances is also sharply dependent on the amount of R_FSH in solution. These observations predicate our assignment of this second group of ^{19}F signals to the second major cluster species.

A plot of (normalized) total integrated signal intensities for the two groups of ^{19}F signals is provided in Figure 8. The ratio of the integrated intensity of the cluster **1** *versus* cluster **4** species increases when the amount of thiol in solution is increased. Addition of a thiol sufficiently acidic to effect terminal ligand substitution (in the presence of H_2S) would also be expected to effect proteolytic cleavage of the (basic) bridging sulfido moieties. Consequently, the monomeric species is refurnished by such a "back-reaction". This observed pattern is, thus, consistent with the assignment of the second major cluster species as a sulfido-bridged oligomer.

In contrast to the substituted cluster **1** species, terminal ligand

(28) (a) Mascharak, P. K.; Smith, M. C.; Armstrong, W. H.; Burgess, B. K.; Holm, R. H. *Proc. Natl. Acad. Sci. U.S.A.* **1982**, *79*, 7056. (b) Armstrong, W. H.; Mascharak, P. K.; Holm, R. H. *Inorg. Chem.* **1982**, *21*, 1699. (c) Armstrong, W. H.; Mascharak, P. K.; Holm, R. H. *J. Am. Chem. Soc.* **1982**, *104*, 4373. (d) Mascharak, P. K.; Armstrong, W. H.; Mizobe, Y.; Holm, R. H. *J. Am. Chem. Soc.* **1983**, *105*, 475. (e) Palermo, R. E.; Holm, R. H. *J. Am. Chem. Soc.* **1983**, *105*, 4310.

(29) Holm, R. H.; Ciurli, S.; Weigel, J. *Prog. Inorg. Chem.* **1990**, *38*, 1 and references therein.

(30) Ellis, A. J.; Golding, R. M. *J. Chem. Soc.* **1959**, 127.

(31) Hammett's equation ($pK_a = pK_a$(thiophenol) $- \rho\sigma$) was employed to calculate an estimated pK_a value. The following constants were used in the Hammett equation: pK_a(thiophenol) = 6.615;[32a] $\rho = 1.81$;[32a] $\sigma_{p-CF3} = 0.53$.[32b]

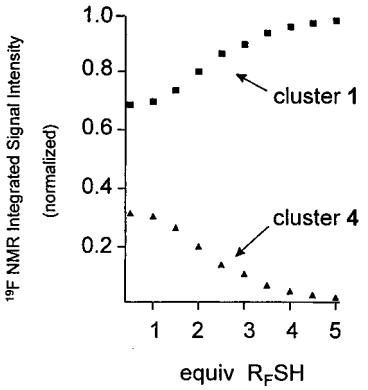

Figure 8. ^{19}F NMR integrated signal intensity for cluster species $[Fe_4S_4(SH)_4]^{2-}$ (**1**) and $\{[Fe_4S_4(SH)_3]_2[Fe_4S_4(SH)_2](\mu\text{-}S)_2\}^{6-}$ (**4**) as a function of equivalents of *p*-$CF_3C_6H_4SH$ added.

substitution of an oligomeric self-condensation product (*e.g.* clusters **2**−**5**) gives rise to a plethora of geometric isomers. Clusters **2**, **3**, and **5** can each give rise to a maximum number of 9, 6, and 8 ^{19}F resonances, *i.e.*, less than the total ^{19}F resonances observed. The sulfido-bridged acyclic tricubane (**4**), however, can generate up to 27 ^{19}F resonances. Therefore, of the conceivable self-condensation products only cluster **4** can possibly account for the number of observed ^{19}F resonances. Hence, this line of inquiry independently supports the ESMS results.

(c) 1 + *p*-$NO_2C_6H_4SH$: ^{1}H NMR Studies. The (aqueous) pK_a value for *p*-$NO_2C_6H_4SH$ (RSH) is 4.5;[32a] it is therefore sufficiently acidic to displace terminal hydrosulfido groups, as discussed above. The ^{1}H NMR spectral changes pursuant to the addition of this acidic arylthiol is shown in Figure 9A−D. The SH resonances decrease significantly in intensity and undergo a detectable chemical shift change upon terminal ligand substitution. Thus upon addition of an equiv of RSH, two (weaker) SH signals are observed at 57.4 and 59.1 ppm in addition to a (stronger) signal which appears as a doublet (48.0 and 48.4 ppm). The relative intensities and the chemical shifts of these signals justify their assignment as the partially substituted oligomeric and monomeric clusters, respectively. The greater extent of splitting of the oligomeric SH resonances upon partial substitution is indicative of a greater anisotropy in the chemical environment of its SH groups; this observation reflects the lower symmetry of this oligomeric structure. Appearance of the free thiol resonances (Figure 9D, marked ∗) upon addition of 4 equiv of RSH is indicative that there is less than 4 equiv of exchangeable SH moieties in solution. This observation is consistent with the suggested self-condensation of **1**, which lowers the number of terminal SH groups.

Comparison with an authentic sample of cluster **7**[33] supports the assignment of 6.20 and 8.90 ppm signals (Figure 9A−D) to the *ortho* and *meta* protons of the aromatic thiolato ligands, respectively.[16] An important caveat to this assignment is that the linewidths for these signals are much larger than those observed in the ^{1}H NMR spectrum of **7** ($\omega_{1/2}$ = 65 and 36 Hz respectively). Addition of excess H_2S, however, does restore the line widths of the 6.20 and the 8.90 ppm signals close to the values expected for **7** (*cf.* Figure 9D−E). Thus these resonances may represent an overlap of two groups of signals, one (group) of which is particularly sensitive to the presence of excess H_2S.[33]

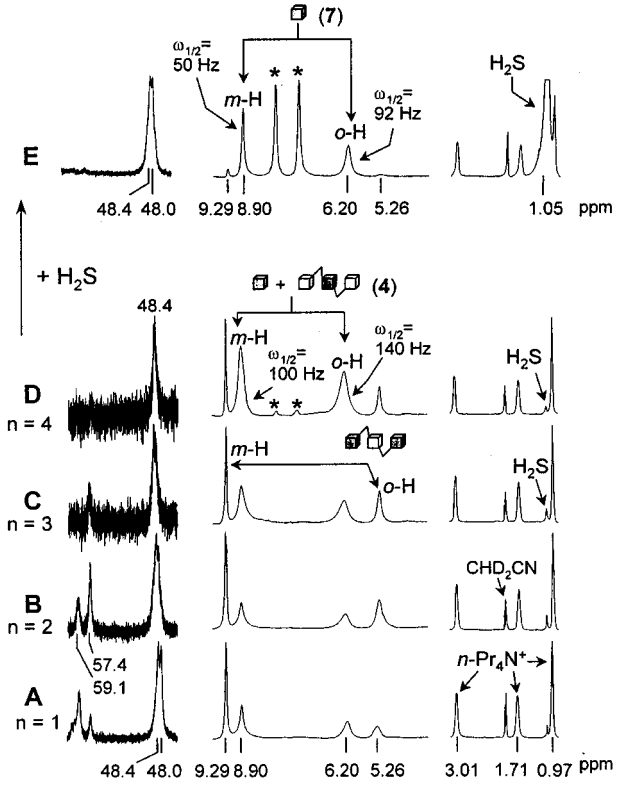

Figure 9. ^{1}H NMR spectral changes (400 MHz) caused by the addition of *n* equiv of *p*-$O_2NC_6H_4SH$ to a CD_3CN solution of $[Fe_4S_4(SH)_4]^{2-}$ (**1**) (A−D), and upon H_2S addition to a solution of **1** + 4 equiv of thiol (E). The signals marked with asterisk (∗) are free thiol resonances. The shaded single cube symbol refers to **7**. The triple cube symbol refers to substituted tricubane **4**; the shading is meant to aid in the distinction between the terminal *versus* the bridging arylthiolate signals (see text).

As shown in Figure 9E, addition of excess H_2S also causes amplification of signals due the free RSH and the terminal hydrosulfido protons of the (partially) substituted cluster **1** species (*i.e.*, 48.0 and 48.4 ppm signals), as well as the disappearance of the resonances at 5.26 and 9.29 ppm. These observations are uniformly consistent with the assignment of 5.26 and 9.29 ppm resonances to the *second* major cluster species. It therefore appears that the second cluster has *two* resonances for *ortho* and *meta* protons each, with one set overlapping with those of the substituted cluster **1** species while the other set is unencumbered (*i.e.*, 5.26 and 9.29 ppm signals). This is solely consistent with the sulfido-bridged acyclic tricubane structural motif of cluster **4**, inasmuch as the *ortho* and *meta* proton chemical shifts of the arylthiolato groups situated on the terminal $[Fe_4S_4]^{2+}$ units should be different from those on the bridging $[Fe_4S_4]^{2+}$ unit (Figure 9C−D). On the basis of relative integrated intensities, it seems reasonable to attribute the 5.26 and 9.29 ppm signals to the *ortho* and *meta* protons of the terminal arenethiolato moieties. The signals for the analogous protons on the bridging $[Fe_4S_4]^{2+}$ unit appear to overlap with the 6.20 and 8.90 ppm signals, which is predominantly due to the *ortho* and *meta* protons of substituted cluster **1** species.

The increase in the relative concentration of cluster **1** to cluster **4** species upon increasing the solution concentration of

(32) (a) De Maria, P.; Fini, A.; Hall, F. M. *J. Chem. Soc., Perkin Trans. 2* **1973**, 1969. (b) Carey, F. A.; Sundberg, R. J. *Advanced Organic Chemistry*, 2nd ed.; Plenum: New York, 1984; Vol. A; p 183 and references therein.

(33) Cluster **7** was generated in CD_3CN solution by the reaction of $[Fe_4S_4(SEt)_4]^{2-}$ with 4 equiv of *p*-$O_2NC_6H_4SH$. The signal broadening in Figure 9D does not arise from differently substituted single cubanes because at this point terminal ligand substitution is complete; further, no such line broadening is observed in the reaction system producing **7**.

the (acidic) arenethiol is also manifest in this set of experiments (Figure 9C−D), even though the overlap of signals makes this observation less vivid than in the case of ^{19}F NMR experimental results (Figure 8). A similar observation was also made upon addition of H_2S (*cf.* Figure 3A,B). Thus addition of a protic acid, whether organic or inorganic, is inimical to cluster **4** species in solution, presumably due to the proteolytic cleavage of the basic sulfido bridges.

Self-Condensation Equilibrium Constant. As indicated above, **1** co-exists with the acyclic tricubane, **4**—the principal self-condensation product—in an H_2S-dependent equilibrium. When the minor species (≲5%; *cf.* Figure 3A) are disregarded, this equilibrium can be defined by eqs 5 and 6. The K_{eq} value

$$3[Fe_4S_4(SH)_4]^{2-} \rightleftarrows \mathbf{4} + 3H_2S \quad (5)$$

$$K_{eq} = \{[\mathbf{4}][H_2S]^3\}/[Fe_4S_4(SH)_4]^3 \quad (6)$$

was determined by an NMR method as described below. The spectral integration values of SH(**1**) and SH(**4**) signals (Figure 3A) were used to calculate the mole fraction values of **1** and **4**, respectively. These mole fractions together with the known total concentration of $[Fe_4S_4]^{2+}$ cores permitted calculation of the solution concentration of **1** and **4**. The solution concentration of H_2S was also determined using ^1H NMR integration. Since the H_2S resonance (1.05 ppm) partially overlaps with an *n*-Pr_4N^+ signal at 0.97 ppm, its estimated value was determined as the *difference* between the total integration of the overlapping signals and the calculated value for the 0.97 ppm signal on the basis of the integral for the unencumbered *n*-Pr_4N^+ resonance at 3.01 ppm. The ratio of the H_2S integral thus obtained to that of the 3.01 ppm *n*-Pr_4N^+ signal yielded the mole fraction of H_2S. The calculated concentration of H_2S based on its calculated mole fraction was then corrected by using Henry's Law.[34] Under these simplifying assumptions, $K_{eq} = 0.1(1)$, in CD_3CN at 298 K, for equilibrium 5. The small value of this equilibrium is a semiquantitative reflection of the aforementioned observations that the self-condensation equilibrium is largely shifted toward **1**. This is in accord with the expectation that the sulfide bridges would be unstable with respect to proteolytic cleavage in the presence of an acid such as H_2S.

Summary. Cluster **1** displays a distinctive solution chemistry while otherwise being a standard $[Fe_4S_4]^{2+}$ cluster in terms of its solid-state structure, redox potential, and spectrophotometric features. The predominant species in solution, single cubane **1**, co-exists in an H_2S-dependent equilibrium with a second (major) cluster species. Detailed examination of the terminal ligand substitution products in acetonitrile solution, using a combination of ESMS, ^1H and ^{19}F NMR spectroscopy, was undertaken. These studies collectively demonstrate that the second cluster is the bridged bis(μ-sulfido) acyclic tricubane **4**. Shown in Figure 10 is a summary of the solution chemistry of cluster **1** as revealed by the studies reported herein. Cluster **1** undergoes self-condensation which liberates H_2S and produces cluster **4** as a major (but not the only) product. This equilibrium is shifted to the left, presumably due to the susceptibility of the (basic) sulfide bridges to proteolytic cleavage. Substitution of the terminal hydrosulfide groups can be achieved by using arenethiols with pK_a values lower than that of H_2S. Addition of increasing amounts of (acidic) arenethiols was also observed to increase the ratio of cluster **1** to cluster **4** species. The same

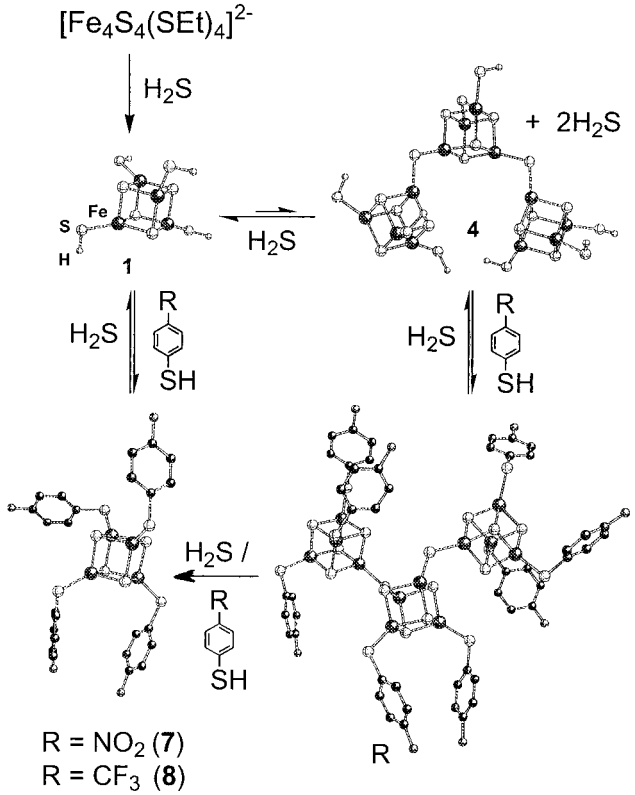

Figure 10. Preparation, self-condensation, and terminal ligand substitution reactions of $[Fe_4S_4(SH)_4]^{2-}$ (**1**). The fully substituted versions of **1** and the sulfido-bridged tricubane **4** are shown; incompletely substituted species (not shown) have been detected.

changes were observed upon addition of excess amounts of H_2S to a solution of substituted cluster **1**. These observations are indicative of the proteolytic cleavage of the (basic) sulfide bridges caused by the added acidic reagents (acidic thiols, H_2S).

Our interest in higher nuclearity Fe−S clusters is spurred by their emergence as a biologically relevant subclass. We have been able to spectroscopically identify a bis(μ-sulfido) linear trimer of $[Fe_4S_4]^{2+}$ units in acetonitrile solutions of cluster **1**. While this is an unprecedented structural motif, it has not yet been identified in any biomolecules. Development of other synthetic routes, amenable to the isolation of higher nuclearity sulfido-bridged Fe−S clusters, is actively under investigation in this laboratory.[4c]

Acknowledgment. This research was supported by NIH Grant GM 28856. We are indebted to Brent M. Segal and Dr. Jeffrey R. Long for crystallographic experiments, to Mihai Azimioara for help with NMR experiments, and to Dr. Alexander Nivorozhkin for critical reading of the manuscript. The Harvard University Department of Chemistry and Chemical Biology Mass Spectrometry Facility is supported by grants from the NSF (CHE-9020043) and NIH (S10-RR08458). We thank Dr. A. Tyler and Dr. E. Larka (University of Minnesota) for useful discussions and experimental assistance in mass spectrometry. H.R.H. gratefully acknowledges a postdoctoral fellowship from Natural Sciences and Engineering Research Council of Canada (1995−1997).

Supporting Information Available: X-ray structural information for (*n*-$Pr_4N)_2$[**1**], including tables of crystal and intensity collection data, positional and thermal parameters, and interatomic distances and angles (12 pages). Ordering information is given on any current masthead page.

IC970412H

(34) The value of Henry's Law constant for H_2S in acetonitrile is 32.9 atm/mol fraction at 25 °C and 759 Torr. This corresponds to a 0.528-(±0.009) M solubility. (Evans, J. F.; Blount, H. N. *Anal. Lett.* **1974**, *7*, 445.)